Load-Frequency Control in a Multi-Source Power System Connected to Wind Farms through Multi Terminal HVDC Systems

Mehdi Tavakoli[a], Edris Pouresmaeil[b,c], Jafar Adabi[d], Radu Godina[e] and João P. S. Catalão[c,e,f,1]

[a] Department of Electrical Engineering, Mazandaran University of Science and Technology, Babol, Mazandaran, Iran
[b] Department of Electrical Engineering and Automation, Aalto University, 02150 Espoo, Finland
[c] INESC-ID, Instituto Superior Técnico, University of Lisbon, 1049-001 Lisbon, Portugal
[d] Faculty of Electrical and Computer Engineering, Babol (Noshirvani) University of Technology, PO Box 484, Babol, Iran
[e] C-MAST, University of Beira Interior, 6201-001 Covilhã, Portugal
[f] INESC TEC and the Faculty of Engineering of the University of Porto, 4200-465 Porto, Portugal

***Abstract*—This paper addresses the wind farm contribution in frequency control during the integration in the power grid. In the proposed model, the wind farm utilizes inertia control and droop control techniques with the purpose of improving the frequency regulation. In order to achieve optimal results, all the parameters of the controllers for the different units in the power grid are obtained by using a particle swarm optimization algorithm (PSO) and by introducing a modified objective function instead of a conventional objective function e.g., Integral Time-weighted Absolute Error (ITAE). Also, different constraints such as reheat turbine, time delay, governor dead band and generation rate constraint (GRC) are considered for thermal and hydro units with the aim of studying a more realistic power system, which is the main contribution of this paper when compared to the other works in this field. It is shown that, in case of a perturbation in power demand, the system frequency will recover quickly and effectively in comparison with the traditional approaches. In addition, a sensitivity test is carried out in a single power grid area in order to examine the effectiveness of the proposed approach. Then, the system is extended to a multi-area power system using a multi-terminal HVDC for further investigation of the suggested strategy. Simulation results are presented in order to assess the performance of the proposed approach in the power system.**

***Index Terms*— Frequency control; particle swarm optimization (PSO); wind farm; multi-terminal HVDC.**

I. Introduction

In general frequency deviation in power system is caused by power imbalance between generation and demand which causes an interchange of power between different areas. In this situation the load frequency control (LFC) is considered to be a major response to this imbalance which aims to return the frequency and interchanging power to their scheduled amounts [1]. The growth of the power demand on the one hand and the increase in the size and intricacy of the power system on the other hand require for new smart systems with diverse energy resources. Researchers are currently trying to find new approaches for LFC in order to keep the frequency and interchanging power in

[1] Corresponding author at Faculty of Engineering of the University of Porto.
E-mail address:catalao@ubi.pt (J.P.S. Catalão).

prearranged amounts against a wide range of disturbances. A critical literature review on the AGC of power systems has been presented in [2], in which have been studied different LFC control aspects. Recently, modern control theory [3], neural networks [4], fuzzy system theory [5] and ANFIS approach [6] are studied with the aim of improving the LFC performance. However, many modern methods such as the ones mentioned above entail a certain degree of complexity which in turn limits their application. Therefore, it is preferred to use classical PI and PID controllers which have advantages like the simple structure and a good performance. Additionally, in some papers intelligent algorithms are used for parameters optimization of PI/PID controllers. In [7] Nanda et al. established Bacterial Foraging Optimization Algorithm (BFOA), which shows a better performance when compared to classical and GA based controllers. In [8] Differential evolution (DE) algorithm is used to optimize the parameters of the controller and the results are compared with BFOA and genetic algorithm (GA). A single area comprising thermal, hydro and gas units is presented in [9] by considering generation rate constraint (GRC) for thermal and hydro units. An optimal output feedback controller which uses only the output state variables is proposed for optimization. The studied system in [9] is extended to a two-area power system in [10] without considering GRC and the DE is used to optimize the parameters of I, PI and PID controllers. Recently, some papers have investigated the contribution of wind farm in frequency control such as [11] and [12]. Wind Energy conversion systems have become remarkable energy resources during the recent years due to the progress in the wind turbine technologies. Thus, offshore wind farms have become an important source of power generation in many countries. An attractive solution for the transferring of this bulk power from a location far away from shore is the voltage source converter based high voltage direct current (VSC-HVDC) system with the purpose of reducing losses and costs. In [13] is shown the method of collecting wind power with multi-terminal HVDC-VSC.

In this paper the wind farm is integrated into a one-area power system introduced in [9], which comprises thermal, hydro and gas units. The inertia and droop control of the wind farm are used to force it to contribute in frequency control of the aforementioned system. In addition, important constraints such as the reheat turbine, time delay, GRC and governor dead band nonlinearity are considered in order to have a more realistic power system. These constraints may affect the system performance and power system dynamic, neglected in many papers like [9 and 10]. A new modified ITAE-based objective function is proposed in this paper in order to decrease the overshoot of the system response as well as minimizing the error [14], [15]. Integral and PID controllers are used for one and two area power systems respectively. Finally, the proposed objective function is minimized

by particle swarm optimization (PSO) algorithm that have shown great success in different types of problems. The performed simulations show a good performance of the presented approach in damping a wide range of disturbances applied to the system.

This paper is organized as follows. The proposed AC area power system is explained in section 2. The contribution of the wind farm in frequency control is presented in section 3. Then, in section 4, a sensitivity analysis is executed in order to show the performance validity of the proposed approach. The proposed method is applied to a multi area power system in Section 5. Finally, the conclusion is provided in section 6.

II. Single area power system for LFC Analysis

A. AC power system

The proposed single area power system comprises a thermal unit with a reheat turbine, a hydro unit and a gas unit. The block diagram of the proposed system is depicted in Fig.1. The participation factors for each unit are considered to specify the amount of the contribution of each unit to the nominal loading. K_{TH}, K_{HY}, K_G are the thermal, hydro and gas units factors, respectively. The summation of these factors must be equal to one. The rest of the system parameters are provided in appendix B.

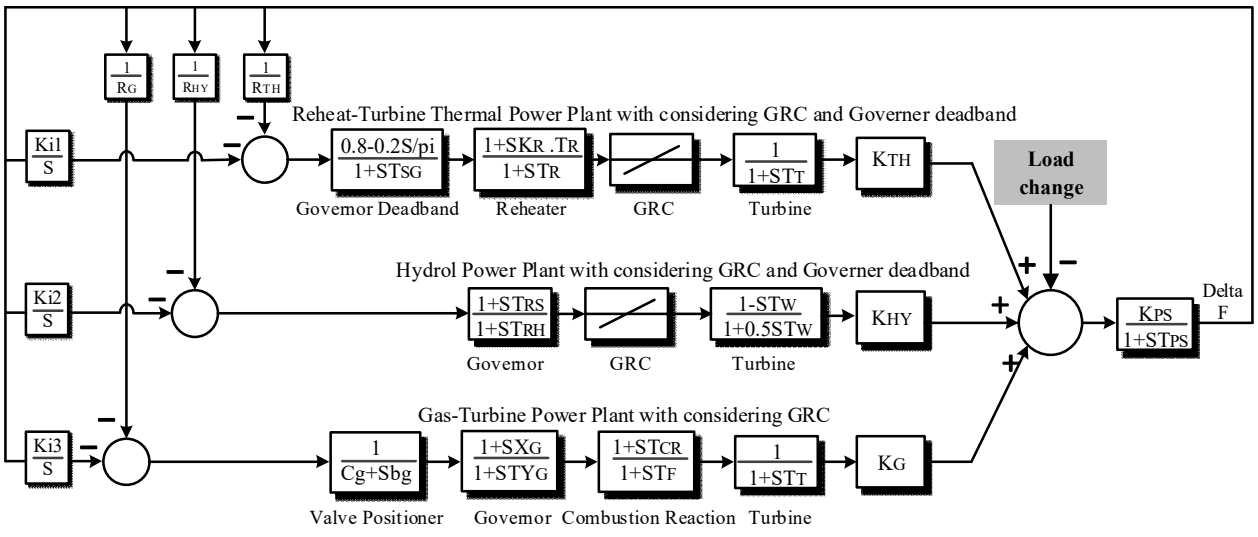

Fig1. The block diagram of the multi-source single area power system.

B. System constraints, optimization and objective function

B.1. System Constraints

In order to have a more realistic power system and with the purpose of carrying out a detailed analysis it becomes necessary to consider the initial requirements and basic physical constraints in the system model. The most important constraints that affect the power system performance are governor dead band nonlinearity, GRC, reheat turbine and time delay [16]. Governor dead band is a continued variation in speed in which the valve position does not alter. Thus, it can increase or decrease the speed before any changes in valve position. Therefore, it can turn the system oscillatory. The transfer function of governor dead band for a thermal unit can be calculated as [17]:

$$G_g = \frac{0.8 - \frac{0.2\pi}{s}}{1 + sT_g} \tag{1}$$

Aside from the governor dead band nonlinearity, GRC is another important practical constraint that should be considered in the analysis. In other words, GRC has a great impact on the dynamic response of the system and its negligence may cause the system to chase large momentary disturbances [18]. Table 1 shows the GRC for thermal and hydro units. ΔP_{gmin} and ΔP_{gmax} are the lower and upper limits respectively. In addition, the time delay is considered 2s in this paper.

Table 1. GRC for thermal and hydro units

$Units$	ΔP_{gmin}	ΔP_{gmax}
$Thermal$	$-0.1\ pu/min$	$0.1\ pu/min$
$Hydro$	$-3.6\ pu/min$	$2.7\ pu/min$

Fig. 2 shows the simulation results (system of Fig.1 with parameters of Appendix B) for frequency deviation response by a 1% step load increase with and without the consideration of GRC. As shown in this figure, GRC effect causes a higher overshoot and longer settling time. In addition, if the parameters obtained during only in the presence of governor dead band effect (without considering time delay and reheat turbine) and applied to the system in which all of the constraints such as the GRC, time delay and reheat turbine are considered, then the system is highly likely to become unstable.

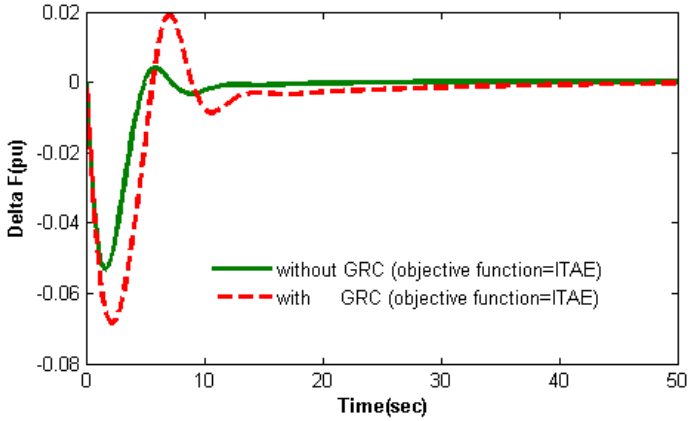

Fig. 2. Frequency deviation response to 1% step load increase.

B. 2. Objective function

The main purpose of the load frequency control is regulating the controllers' parameters in order to keep the frequency and the interchanging power in their scheduled amounts. For this reason, it is required to define an objective function in order to satisfy the desired specifications such as lower overshoot, fast settling time and lower error. The integral time multiplied absolute error (ITAE) in (2) is generally used as an objective function in many previous analyses [19] and is given by:

$$ITAE = \int_0^{t_{sim}} t|e(t)|\,dt \tag{2}$$

where e(t) is the system error. As mentioned in [19], ITAE have the ability to decrease the settling time but it is unable to decrease the overshoot properly. For this reason, a modified objective function (J_{new}) is presented in this paper, which can reduce the overshoot of the system response as well as decreasing its settling time.

$$J_{new} = w_1\left[\int_0^{t_{sim}} t|\Delta F_i|\,dt + \int_0^{t_{sim}} t|\Delta P_{tie}|\,dt\right] + w_2[Overshoot(|\Delta F_i|) + Overshoot(\Delta P_{tie})] \tag{3}$$

where, Δf is the frequency deviation, ΔP_{tie} is the interchanging power between areas, w_1 and w_2 are the weighting factors and t_{sim} is the simulation time.

Fig. 3 shows the simulation result for the single-area power system depicted in Fig. 1 for both conventional ITAE and modified (J_{new}) objective functions. As shown in this figure, it is evident that the system overshoot is considerably reduced by the proposed J_{new} objective function. However, the system undershoot has slightly decreased. Of course, it is possible to create a compromise between the overshoot and undershoot by changing w_1 and w_2.

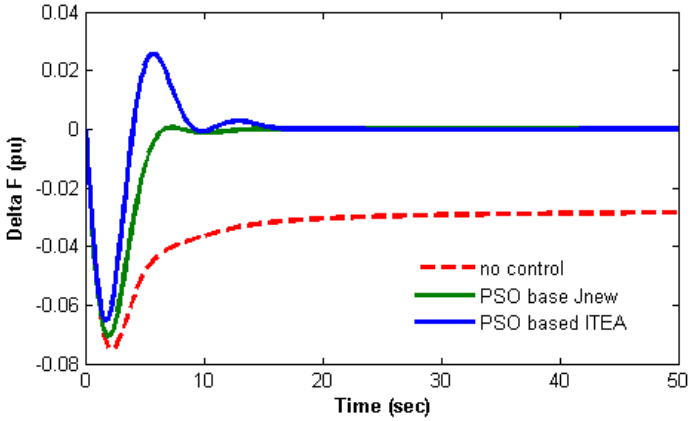

Fig. 3. Frequency deviation response to 1% step load increase.

III. Contribution of wind farms in the frequency control

A. Wind power

During recent years the wind power generation is one of the most important sources of renewable energy due to technical advancements in power converters, efforts to reduce the dependence on fossil fuels, environmental considerations and cost effectiveness. Many countries around the world which have potential wind power are determined to use high penetration level of wind power, not only as a means to reduce CO_2 emissions but also as an interesting economic alternative to the consumption of finite resources.

Wind generated power depends on several factors. The mechanical power of wind turbine is equal to [20]:

$$P_W = \frac{1}{2}\rho A_r C_p V_W^3 \tag{4}$$

$$C_p = (0.44 - 0.0167\beta)\sin\left[\frac{\pi(\lambda - 3)}{15 - 0.3\beta}\right] - 0.018(\lambda - 3)\beta \tag{5}$$

where P_m is the wind mechanical power, ρ is the air density $(\frac{Kg}{m^3})$, A_r is the blades swept area (m^2), V_W is the wind speed and C_P is a function of both speed tip ratio (λ) and blade pitch angle (β). As the mechanical power is related to β, this relation can be used to reserve power. In practice, this work is done by increasing β to reserve power and decreasing β to release power.

B. Wind farm contribution to frequency control

In conventional power plants synchronous generators are connected directly to the power system. It means that there is a coupling between the output active power of the generators and the power system frequency. This is known as the "natural" inertial response of the generator that contributes to frequency stabilization. In variable speed wind turbine there is an electrical decoupling between the wind turbines and the grid due to the intermediate DC voltage bus. Therefore, a significant amount of kinetic energy that is stored in the rotating mass of their blades will not contribute to the inertia of the grid. However, it is possible to use the "hidden inertia" of the wind turbines by adding a control loop. Additionally, variable speed wind turbine has the ability to operate in a wide range of speed changes and it's generator speed can drop to as low as 0.7 PU speed, while conventional unit speed can only drop to as low as 0.95 PU. Hence, from two installations of the same rating and the same H, the variable speed wind turbines would have several times more kinetic energy than the conventional installation and this energy can be used to provide primary frequency control support to the grid in the event of a load/generation mismatch [21], [22]. In addition, a comparison of frequency response characteristics of conventional power plant with wind power plant is presented in [12] by increasing the load demand. The conventional power plants need 4s-25s and 20s-68s for the response and settling time respectively in order to supply the demand power with the aim of balancing the entire system, whereas wind turbine's response and settling time are 3s-9s and 8s-38s for the response and settling time, respectively. Consequently, wind turbines can supply power to the system during this transition time to meet the increased demand and stabilize the frequency [21]. Inertia control and droop control are used in this paper to make the wind farm contribute in frequency control.

B. 1. Inertia control of wind farm

The inertia response contribution will be determined by the control-loop gain, which is defined by the wind turbines kinetic energy [23]-[24]. The kinetic energy stored in the spinning blade of the wind turbine has a considerable amount of energy. However, the wind turbine and grid are decoupled from each other because there is a DC link between them which prevents the wind contribution in frequency control. Thus, the inertia control is used in this paper to reduce the maximum frequency change rate [25]. The amount of active power (P_{in}) generated by the inertia control is equal to:

$$P_{in} = -k\frac{df}{dt} \tag{6}$$

where k is the constant that its maximum amount is equal to 2H (H is the turbine inertia constant). A negative sign in this equation represents the action of reducing the frequency. Therefore, the reference power for the wind farm would be changed according to Fig. 4.

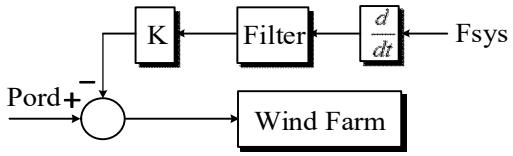

Fig.4. Control loop for HVDC rectifier with inertia control.

B. 2. Droop control of wind farm

By using droop control the steady-state frequency response will be determined by the droop gain of the frequency control loop. The concept is similar to the frequency droop in the speed governor of a synchronous generator. Wind farms can successfully participate in primary frequency response by a frequency-power droop when the system has a load or a generation change. The prime mover (wind turbine) will change its output through its pitch controller [11]. The idea is the same as the frequency droop in the turbine governor of a synchronous generator. It is essential to use this control, especially in a system with high wind penetration. Otherwise, the system frequency deviation will be high in the presence of load changes. For this reason, the wind farm maintains a small portion of its generated power (usually about 10%) as a reserve in order to inject into the system when it is necessary. This action is done by adjusting the pitch angle. By using this control the amount of active power generated by droop control is equal to:

$$P_{in} = -\frac{\Delta f}{R_{WF}} \tag{7}$$

where R_{WF} is a parameter which imitates the governor speed regulation in conventional power plants. Therefore, the reference power for the wind farm would be changed according to Fig. 5.

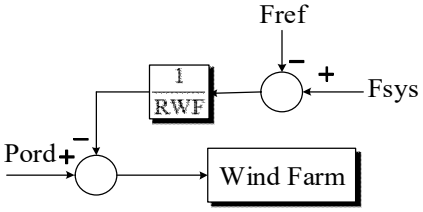

Fig. 5. Control loop for HVDC rectifier with droop control.

B. 3. Connection of wind farm to the power system

Fig. 6 shows the connection of a wind farm to the supposed single area power system (Fig. 1) through a HVDC line. The linearized model considered for load frequency of the system is depicted in Fig. 7. With the aim of simplifying, the transfer function of the wind farm and HVDC are represented by a first order lag function. K_{TH}, K_{HY}, K_G and K_{WF} are the thermal unit, hydro unit, gas unit and wind power unit participation factors, respectively. Such factors specify the amount of the contribution of these types of units to nominal loading. The summation of these factors must be equal to one. The rest of the system parameters are provided in appendix B. According to the grid code [26], when the difference between reference frequency and system frequency becomes more than $4 \times 10^{-4} pu$, the inertial control and droop control will be activated to make the wind farm assist in frequency control. Figs. 8 and 9 show the extra generated power by all units (thermal, hydro, gas and wind farm) and the system frequency, respectively, in response to 1% step load increase and for different states of wind farm contributions (only Inertia control, only droop control, combination of both inertia and droop control).

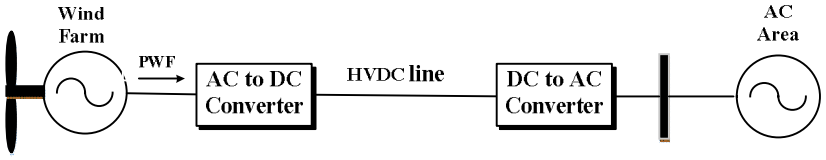

Fig.6. Wind farm connection to AC area through HVDC line.

As it is evident from Fig. 9, by using only the inertia control of the wind farm the system frequency has demonstrated an improvement in minimum frequency from -0.064 to-0.057. However, the rise time has slightly increased. While considering only the droop control for the wind farm, not only the minimum frequency is improved from -0.064 to-0.06, but also the settling time and rise time is significantly decreased. Finally, by using both inertia and droop control of the wind farm, the minimum frequency has grown from -0.064 to -0.052. Besides, the settling time and rise time are noticeably decreased. Therefore, by utilizing both inertia and droop control simultaneously, the wind farm can effectively contribute in frequency control.

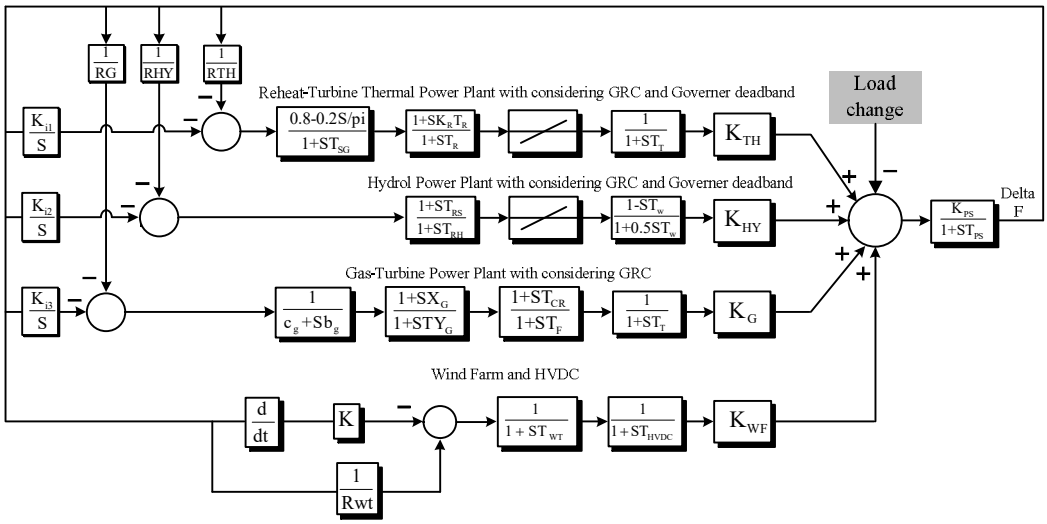

Fig. 7. Block diagram of the multi-source single area power system.

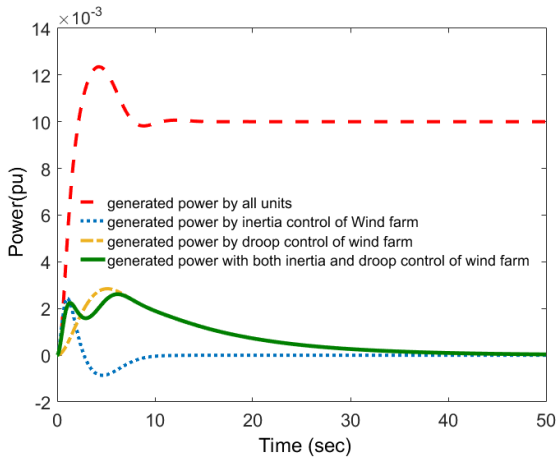

Fig. 8. Extra generated power in response to 1% step load increase with different control strategy.

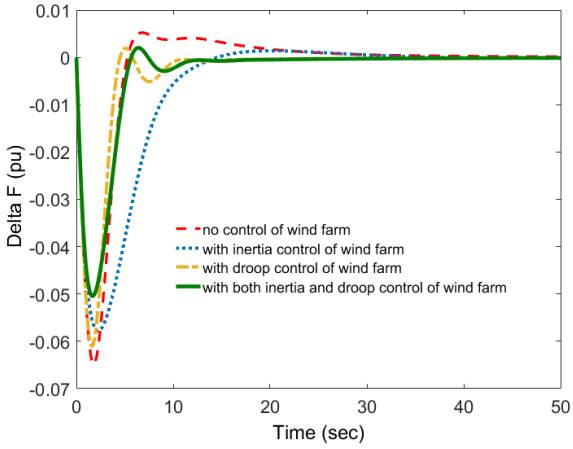

Fig. 9. Frequency deviation response to 1% step load increase with different control strategy

Table 2. Sensitivity analysis.

$Parameters\ variation$	$Change\%$	$PSO\ optimized\ controller\ parameters$			$ITAE\ with\ proposed\ approach$	$ITAE\ with\ optimal\ control$[9]
		k_{i1}	k_{i2}	k_{i3}		
All Nominal	0	0.1368	0.0114	-0.1149	0.5447	0.9934
Loading Condition	-25	0.1379	0.0128	-0.0955	0.3919	1.0116
	+25	0.1380	0.0124	-0.1113	0.7189	0.9762
T_{SG}	-25	0.1382	0.0127	-0.1019	0.5432	0.9955
	+25	0.1379	0.0126	-0.1049	0.5517	0.9986
T_{GH}	-25	0.1375	0.0131	-0.1007	0.5413	0.9896
	+25	0.1372	0.0133	-0.1044	0.5536	0.9971
T_R	-25	0.1451	0.0394	-0.1707	0.6032	0.7902
	+25	0.1517	-0.0290	-0.0628	0.5860	1.1791
T_T	-25	0.1379	0.0133	-0.0965	0.5300	0.9716
	+25	0.1344	0.0146	-0.1050	0.5708	1.0165
T_{RH}	-25	0.1385	0.0163	-0.1043	0.5352	0.9277
	+25	0.1130	0.0276	-0.0566	0.7652	1.0362
T_W	-25	0.1357	0.0136	-0.0992	0.5454	1.0129
	+25	0.1362	0.0134	-0.1185	0.5992	0.9947
T_{CD}	-25	0.1370	0.0127	-0.1105	0.5691	1.0117
	+25	0.1383	0.0119	-0.1104	0.5699	1.0218

IV. Sensitivity analysis

In this section, a sensitivity analysis is carried out in order to examine the stability of the proposed approach. The effects of changing load and system parameters on the dynamic response of the power system are investigated. Each load and system parameters is changed by ±25% of their nominal value and their effect is analyzed on the system response. The controller's gain (optimized by PSO) and ITAE calculated in response to 1% step load increase are shown in table 2. In addition, for the purpose of comparison, ITAE obtained from proposed method in [9] is also provided in this table. It is shown that the effect of the changing load and system parameters on dynamic performance of the system is almost negligible. Hence, it can be concluded that the proposed approach is stable in different conditions and the controller parameters obtained at nominal condition do not need to be changed when a wide range of variation is applied on the load and system parameters. Additionally, the frequency deviation at the presence of load change, thermal unit governor time constant change and thermal unit turbine time constant change are depicted in Figs. 10, 11 and 12, respectively. It is evident from these figures that the applied variations hardly change the system response.

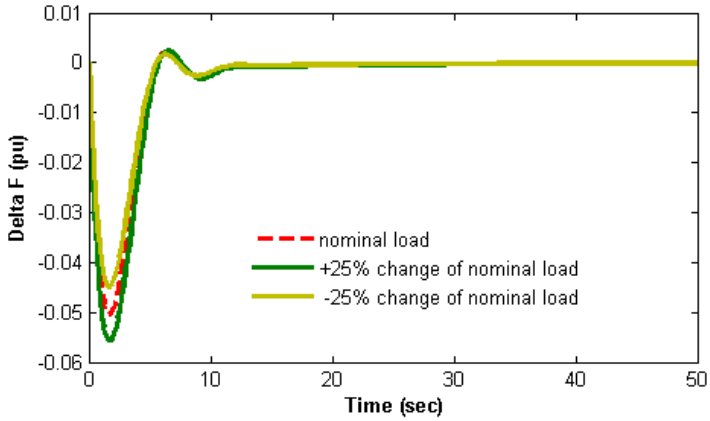

Fig. 10. Frequency deviation response to 1% step load increase with varying load conditions.

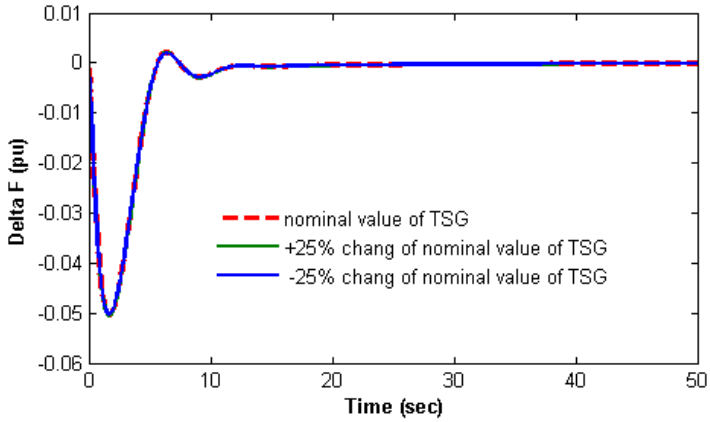

Fig. 11. Frequency deviation response to 1% step load increase with varying governor time constant.

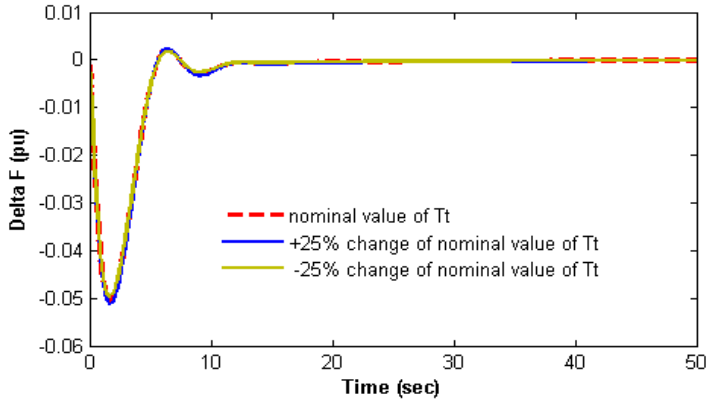

Fig. 12. Frequency deviation response to 1% step load increase with varying turbine time constant.

V. Extension to multi-area power system

The development of the wind energy in the future would lead to the growth of large capacity offshore wind farms in remote locations from terrestrial grid where the wind energy has a high potential and enough space for the installation of such a huge offshore wind farm. Integration of these offshore wind farms constructed in remote distances from the terrestrial grid require an effective transmission network that needs long and robust cable connection. In addition, the developing of a transnational network in the future which will link different countries increases the length of the required transmission cables which raise the system costs. Therefore, an efficient transmission network that is economically viable is needed for the integration of the wind farms in near future. The best solution for this problem is VSC based HVDC that is proposed in many works [27].

In order to extend the studied system into a multi-area power system, two wind farms are connected to two AC areas which are connected by a tie-line to each other according to Fig. 13. The two wind farm are also connected with a HVDC line. This topology is one of the best existing ones to connect wind farms and AC areas since it can withstand different faults and needs less breaker operations in relation to other topologies. However, this solution requires more cable [28]. For instance, in case of a fault occurrence at HVDC line connecting the wind farm 1 and AC area 1, the generated power by the wind farm 1 can be injected to the AC area 2 through a DC line between wind farms.

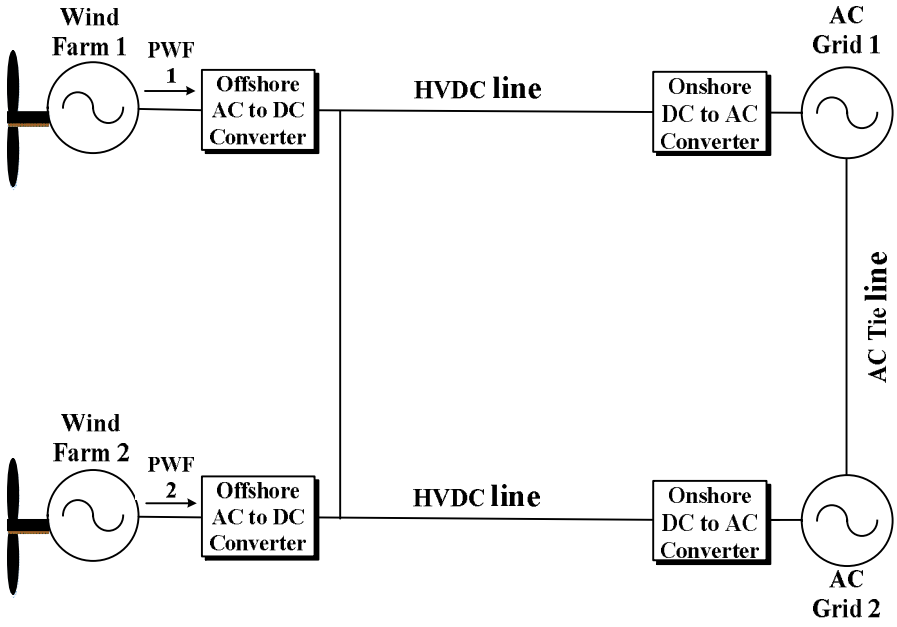

Fig. 13. The proposed topology for connecting of two-area power system to a wind farm using MTDC.

Each AC area comprise thermal a unit, a hydro unit and a gas unit. The transfer function of the proposed system is shown in Fig. 14 and its parameters are provided in appendix B. With the purpose of simplicity, the transfer function of the wind farm and HVDC are represented by a first order lag function. All of the system constraints such as reheat turbine, time delay, GRC and governor dead band are considered in the model to have a more realistic power system. In addition, the PID controller is used since it is one of the most famous feedback controllers and its parameters have been optimized by PSO algorithm. Application of the PID controller in this system reduces the settling time due to its proportional controller and creates a zero steady state error due to its integral controller. It also increases stability, improves the transient state and reduces the overshoot because of its derivative controller. According to Eq. 3, the objective function for the two area power system is equal to:

$$J_{new} = w_1 \left[\sum_{i=1}^{2} \int_0^{t_{sim}} t|\Delta F_i|\, dt + \int_0^{t_{sim}} t|\Delta P_{tie}|\, dt \right] + w_2 \left[\sum_{i=1}^{2} Overshoot(|\Delta F_i|) + Overshoot(\Delta P_{tie}) \right] \quad (8)$$

A. System response to 1% step load increase in AC area 1

A 1% step load increase is applied to the AC area 1 in order to analyze the dynamic performance of the two-area system. Fig.15 shows the extra generated power by wind farms using both inertia and droop control. Fig. 16 shows the extra generated power by all units in response to 1% load increment with and without the wind farm contribution in meeting power demand increment. The system responses are obtained under two different cases and the results are shown in Figs. 17 to 19. In case 1, the system response is obtained without the wind contribution under conventional ITAE objective function. In case 2, the system response is obtained with the wind contribution in frequency control using the modified objective function (J_{new}). Additionally, Table 3 shows the percentage of the improvement in overshoot, undershoot and integral of Δ_f in both areas. Figs. 17 and 18 illustrate the frequency deviations in area 1 and 2 for both cases, respectively.

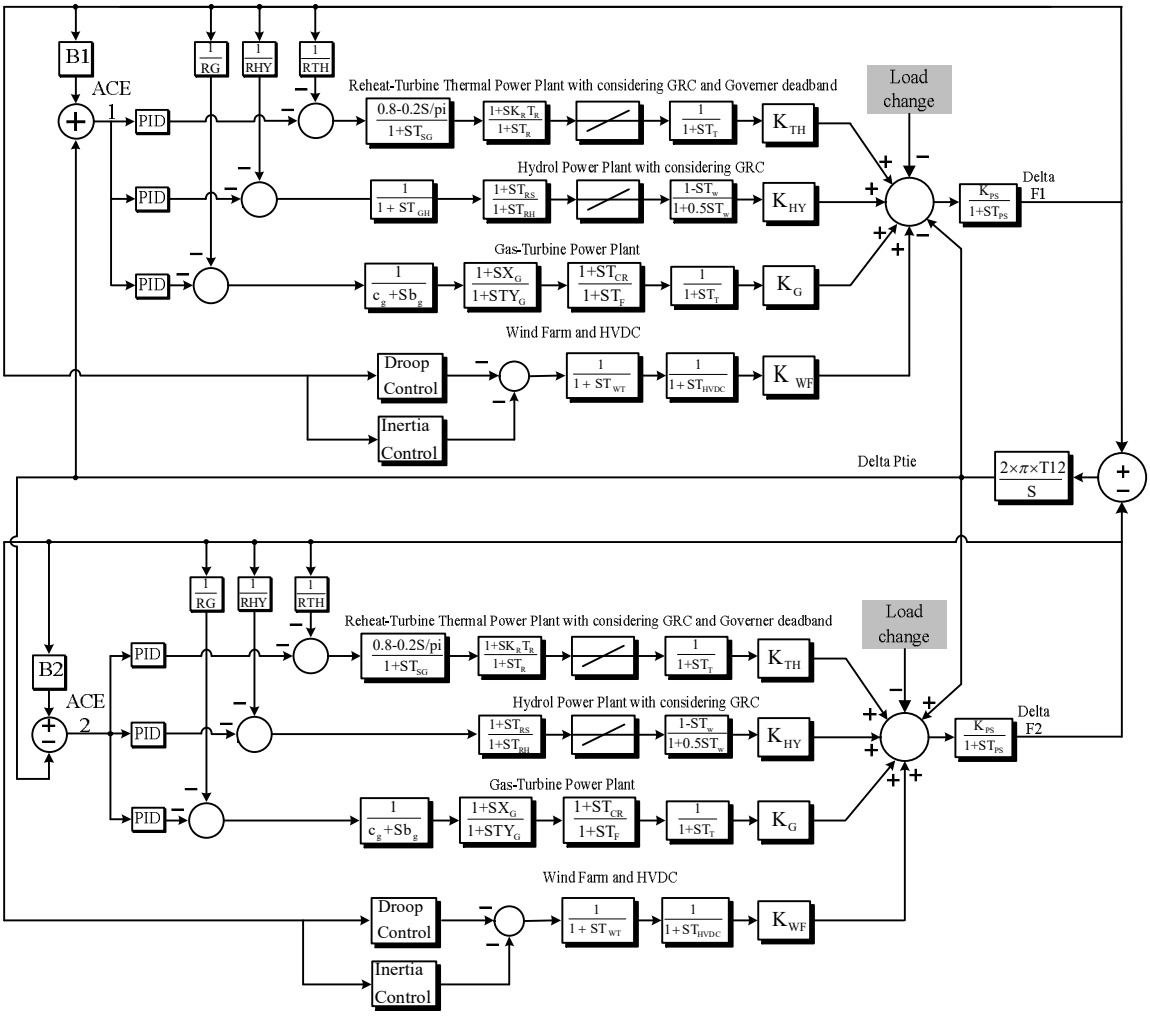

Fig. 14. Transfer function of a two-area power system.

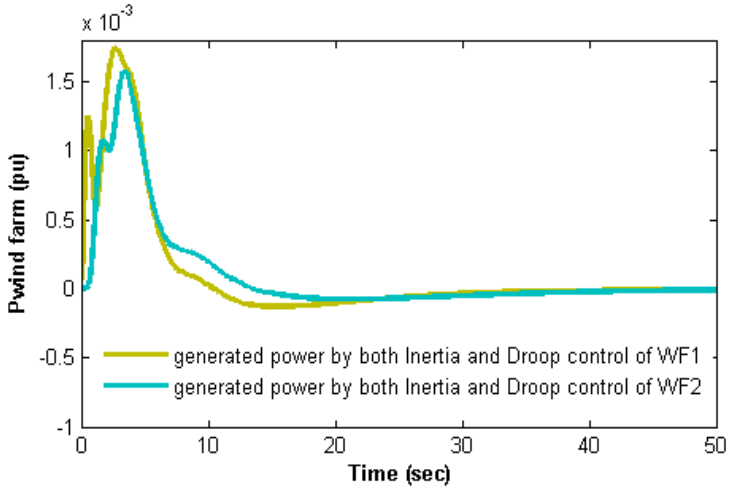

Fig. 15. Extra generated power by wind farms in response to 1% step load increase in area 1.

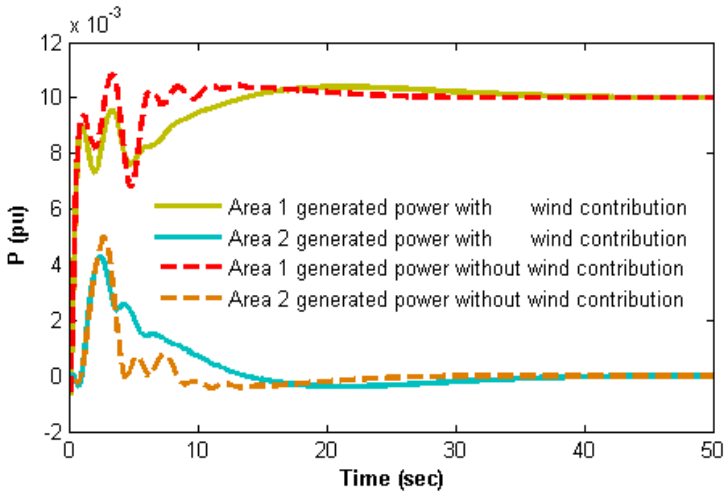

Fig. 16. Extra generated power by all units to 1% step load increase in area 1 with and without wind farm contribution.

Table 3. System response to 1% step load increase in area 1.

Parameters	$\Delta f1$		Improvement	$\Delta f2$		Improvement
	Case1	Case2		Case1	Case2	
Overshoot	0.014	0.002	85.7%	0.008	0.001	87.5%
Undershoot	-0.027	-0.023	14.8%	-0.028	-0.021	25%
$\int_0^{Tsim} \lvert\Delta f\rvert dt$	0.0761	0.0587	22.9%	0.0643	0.0490	23.7%

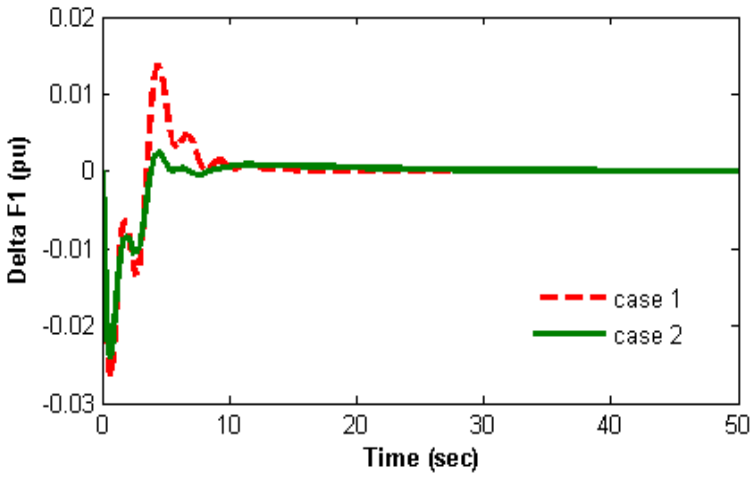

Fig. 17. Frequency deviation of area 1 to 1% step load increase in area 1.

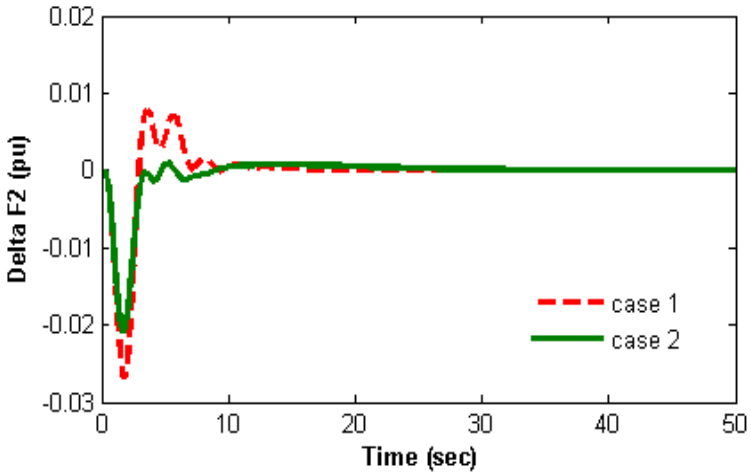

Fig. 18. Frequency deviation of area 2 to 1% step load increase in area 1.

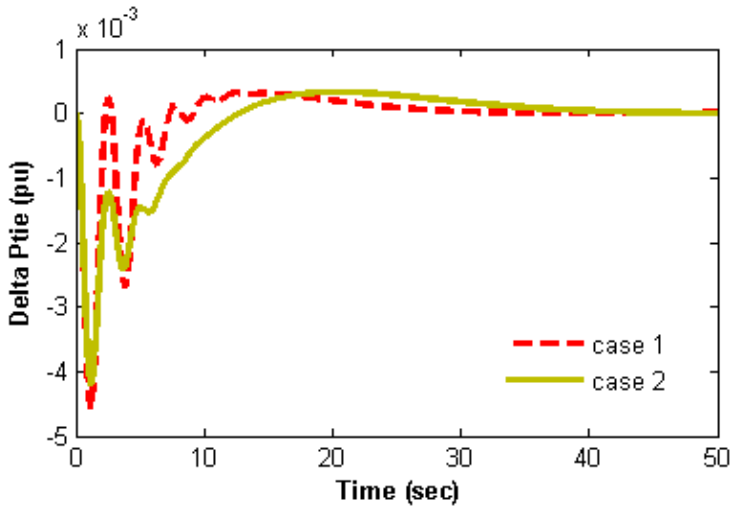

Fig. 19. Tie line power deviation to 1% step load increase in area 1.

In addition, Fig. 19 shows the deviation of the tie line power. According to Table 3 and Figs. 17 and 19, overshoot, undershoot and frequency deviation in case 2 have decreased significantly when compared to the case 1. Moreover, the settling time of frequency have decreased in both areas in relation to case 1. It is also evident from Figs. 16 to 19 that using the suggested policy helps the system to reach to the steady state with a lower fluctuation.

B. System response to 1% step load increase in area 1 and 2% step load increase in Area 2

In order to further the study of the proposed approach and to investigate its performance under different conditions, a 1% step load increase in area 1 and 2% step load increase in area 2 are applied at $t = 0$. Fig. 20 and Fig. 21 show the extra generated power by wind farms and all units, respectively, in response to these load increases.

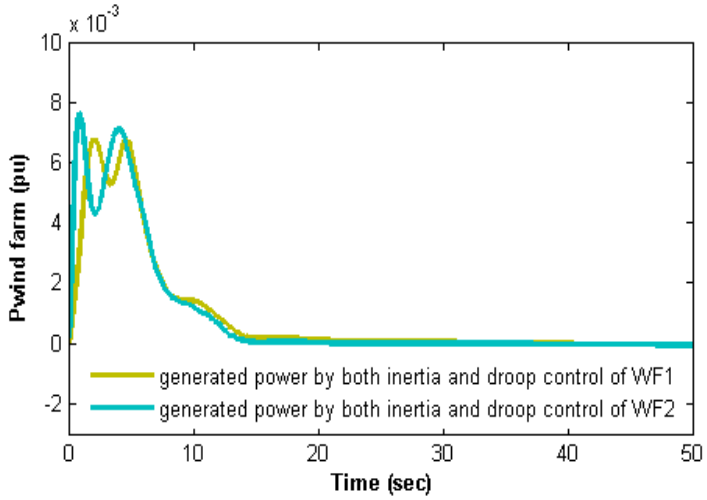

Fig. 20. Extra generated power by wind farms to 1% step load increase in area 1 and 2% step load increase in area 2.

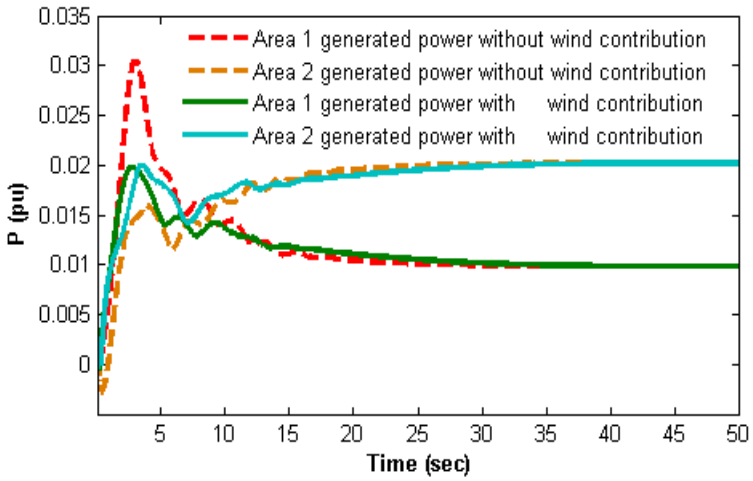

Fig. 21. Extra generated power by all units to 1% step load increase in area 1 and 2% step load increase in area 2.

The system responses are obtained under 2 cases as in section 5.1 and the results are shown in Figs. 22 to 24. Table 4 shows the percentage of the improvement in overshoot, undershoot and integral of Δ_f in both areas. Figs. 22 and 23 illustrate the frequency deviations in area 1 and 2, respectively. In addition, Fig. 24 shows the deviation of the tie line power for the two mentioned cases.

According to Table 4 and Figs. 22 and 23, the overshoot, undershoot and frequency deviation in case 2 have decreased considerably when compared to the case areas 1 in 2. Besides, the settling time of the frequency was reduced in both areas rather than in case 1. It is also obvious from Figs. 21 to 24 that the system reaches the steady state with lower oscillations.

Table 4. System response to 1% step load increase in area 1 and 2% step load increase in area 2 simultaneously.

parameters	$\Delta f1$		Improvement	$\Delta f2$		Improvement
	Case1	Case2		Case1	Case2	
$Overshoot$	0.008	0.003	62.5%	0.008	0.004	50%
$Undershoot$	-0.105	-0.073	30.4%	-0.117	-0.08	31.6%
$\int_0^{Tsim} \lvert\Delta f\rvert dt$	0.3398	0.2588	23.8%	0.3780	0.2728	27.8%

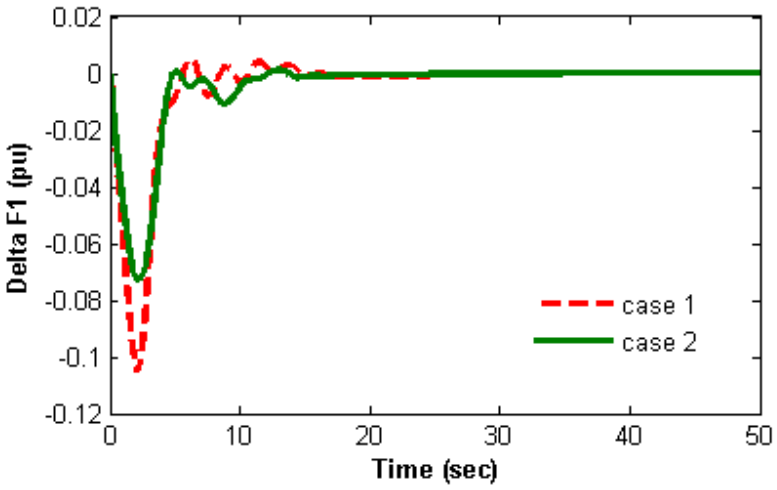

Fig. 22. Frequency deviation of area 1 to 1% step load increase in area 1 and 2% step load increase in area 2.

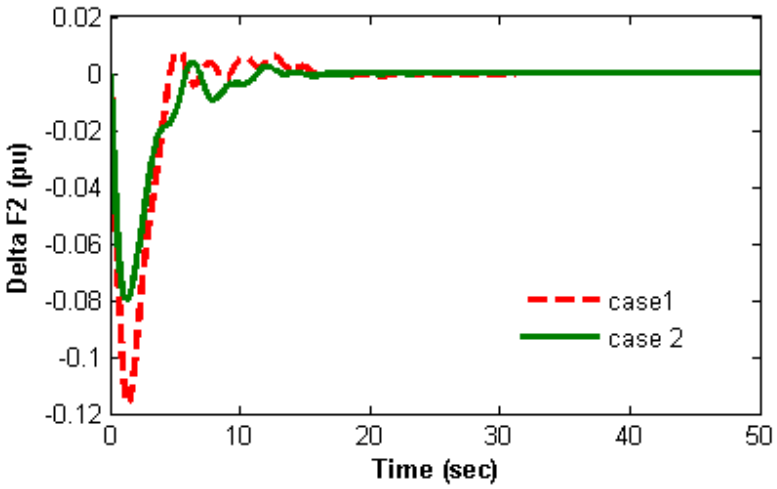

Fig. 23. Frequency deviation of area 2 to 1% step load increase in area 1 and 2% step load increase in area 2.

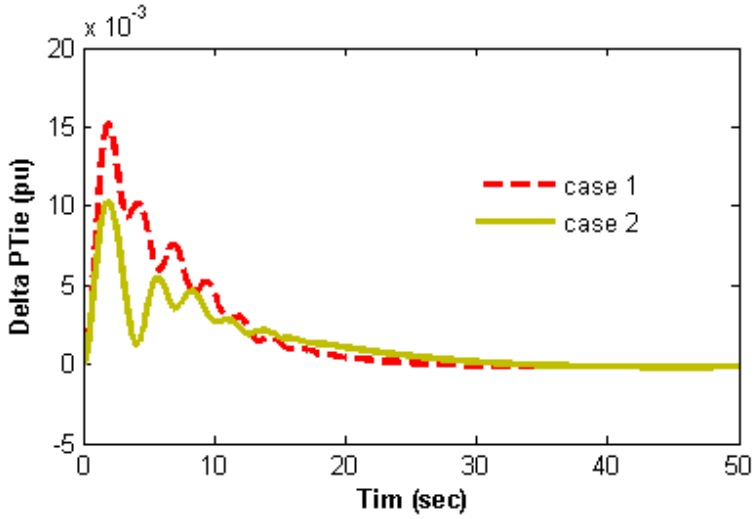

Fig. 24. Tie line power deviation to 1% step load increase in area 1 and 2% step load increase in area 2.

VI. Conclusion

In this paper, the wind power generation was incorporated to a power system comprising thermal, hydro and gas units with the aim of contributing in frequency control. The system constraints such as GRC, reheat turbine, time delay and governor dead band were also considered in order to study a more realistic power system. In general wind farms do not contribute in frequency control due to converters that decouple them from grid. In order to utilize the wind farm ability in frequency contribution, inertia control and droop control were used in this paper. With the purpose of analyzing the proposed approach, a single area was considered and a sensitivity test was performed

with the aim to demonstrate its stability. The simulations revealed that the load and the parameters' changes had a negligible effect on the dynamic performance of the system. The system was extended to a two-area power system afterwards. In both single and two areas system, the controllers' parameters were optimized by a PSO algorithm by introducing a new modified objective function. The results showed that the system response with the contribution of the wind farm in frequency control has noticeably improved, since not only the overshoot and interchanging power have decreased, but also the undershoot or minimum frequency have improved significantly. Also, the settling time decreased and the system achieved the steady state more smoothly and with a lower fluctuation. It was assumed that in the simulations performed in this paper the wind speed was constant. However, in real conditions, the wind turbines suffer from uncertainty and fluctuations in their generated power. Thus, it will be useful to consider such a challenge in an upcoming work in frequency control management.

Acknowledgment

This work was supported by FEDER funds through COMPETE 2020 and by Portuguese funds through FCT, under Projects SAICT-PAC/0004/2015 - POCI-01-0145-FEDER-016434, POCI-01-0145-FEDER-006961, UID/EEA/50014/2013, UID/CEC/50021/2013, UID/EMS/00151/2013 and SFRH/BPD/102744/2014. Also, the research leading to these results has received funding from the EU Seventh Framework Programme FP7/2007-2013 under grant agreement no. 309048.

References:

[1] Tan W. Unified tuning of PID load frequency controller for power systems via IMC. IEEE Trans Power System 2010; 25(1): 341-350.

[2] Ibraheem, Kumar P, Kothari D P. Recent philosophies of automatic generation control strategies in power systems. IEEE Trans Power System 2005; 20(1): 346-357.

[3] Shoults R R, Jativa Ibarra J A. Multi area adaptive LFC developed for a Comprehensive AGC simulation. IEEE Trans Power System 1993; 8(2): 541-547.

[4] Chaturvedi D K, Satsangi P S, Kalra P K. Load frequency control: a generalized neural network approach. Int. J. Elect. Power Energy System 1999; 21(6): 405-415.

[5] Ghosal S P. Optimization of PID gains by particle swarm optimization in fuzzy based automatic generation control. Electrical Power System Research 2004; 72: 203–212.

[6] Khuntia S R, Panda S. Simulation study for automatic generation control of a multi-area power system by ANFIS approach. Applied Soft Computing 2012; 12(1): 333-341.

[7] Nanda J, Mishra S, Saikia L C. Maiden application of bacterial foraging based optimization technique in multiarea automatic generation control. IEEE Trans Power System 2009; 24(2): 602-609.

[8] Rout U K, Sahu R K, Panda S. Design and analysis of differential evolution algorithm based automatic generation control for interconnected power system. Ain Shams Engineering Journal 2013; 4(3): 409-421.

[9] Singh Parmar K P, Majhi S, Kothari D P. Load frequency control of a realistic power system with multi-source power generation. Int. J. Elect. Power Energy System 2012; 42(1): 426–433.

[10] Mohanty B, Panda S, Hota P K. Controller parameters tuning of differential evolution algorithm and its application to load frequency control of multi-source power system. Int. J. Elect. Power Energy Systems 2014; 54: 77-85.

[11] Yingcheng X, Nengling T. Review of contribution to frequency control through variable speed wind Turbine. Renewable Energy 2011; 36(6): 1671-1677.

[12] Miao Zh, Fan L, Osborn D, Yuvarajan S. Wind Farms with HVDC Delivery in Inertial Response and Primary Frequency Control. IEEE Trans Energy Conversion 2010; 25(4): 1171-1178.

[13] Khenar M, Adabi J, Pouresmaeil E, Gholamian A, Catalão JPS. A control strategy for a multi-terminal HVDC network integrating wind farms to the AC grid. Int. J. Elect. Power Energy System 2017; 89: 146-155.

[14] Pouresmaeil E, Funsho Akorede M, Montesinos-Miracle D, Gomis-Bellmunt O. Hysteresis Current Control Technique of VSI for Compensation of Grid-connected Unbalanced Load. Electrical Engineering 2014; 96: 27-35.

[15] Pouresmaeil E, Montesinos-Miracle D, Gomis-Bellmunt O. Control Scheme of Three-level H-bridge Converter for Interfacing Between Renewable Energy Resources and AC Grid. in Proc. 14th IEEE Proceedings of the European Conference on Power Electronics and Applications (EPE), pp. 1-9, Aug. 2011.

[16] Golpîra H, Bevrani H. Application of GA optimization for automatic generation control design in an interconnected power system. Energy Conversion and Management 2011; 52(5): 2247-2255.

[17] Gozde H, Taplamacioglu M C. Automatic generation control application with craziness based particle swarm optimization in a thermal power system. Int. J. Elect. Power Energy Systems 2011; 33(1): 8–16.

[18] Moon Y H, Ryu H S, Lee J G, Song K B, Shin M C. Extended integral control for load frequency control with the consideration of generation-rate constraints. Int. J. Elect. Power Energy System 2002; 24(2): 263-269.

[19] Härtel P, Vrana T K, Hennig T, von Bonin M, Wiggelinkhuizen E J, Nieuwenhout F D J. Review of investment model cost parameters for VSC HVDC transmission infrastructure. Electric Power Systems Research 2017; 151: 419-431.

[20] Mauricio J M, Marano A, Gomez-Exposito A, Ramos J L M. Frequency regulation contribution through variable-speed wind energy conversion system. IEEE Trans Power System 2009; 24(1): 173–180.

[21] Lee D J, Wang L. Small-Signal Stability Analysis of an Autonomous Hybrid Renewable Energy Power Generation/Energy Storage System Part I: Time-Domain Simulations. IEEE Trans Energy Conversion 2008; 23(1): 311-320.

[22] Mehrasa M, Godina R. Pouresmaeil E, Vechiu I, Rodriguez R L, Catalão J P S. Synchronous active proportional resonant-based control technique for high penetration of distributed generation units into power grids. IEEE Proceedings Innovative Smart Grid Technologies Conference Europe (ISGT-Europe), 2017.

[23] Kayikci M, Milanovic J V. Dynamic contribution of DFIG-based wind plants to system frequency disturbances. IEEE Trans Power System 2009; 24(2): 859–867.

[24] Pouresmaeil E, Mehrasa M, Godina R, Vechiu I, Rodriguez R L, Catalão J P S. Double synchronous controller for integration of large-scale renewable energy sources into a low-inertia power grid. IEEE Proceedings Innovative Smart Grid Technologies Conference Europe (ISGT-Europe), 2017.

[25] Remtharan G, Ekanayake J B, Jenkins N. Frequency support from doubly fed induction generator wind turbine. IET Renew Power Generation 2007; 1(1): 3-9.

[26] Ancillary Service to be delivered in Denmark Tender Condition. ENERGYNET.DK 2011.

[27] Mehrasa M, Pouresmaeil E, Zabihi S, Vechiu I, Catalão J P S. A multi-loop control technique for the stable operation of modular multilevel converters in HVDC transmission systems. International Journal of Electrical Power & Energy Systems 2018; 96: 194–207.

[28] Gomis-Bellmunt O, Liang J, Ekanayake J, King R, Jenkins N. Topologies of multi-terminal HVDC-VSC transmission for large offshore wind farms. Electric Power Systems Research 2011; 81(2): 271–281.

Appendix A: Nomenclature

ACE	area control error
P_{rt}	rated capacity of the area, MW
f	nominal system frequency, Hz
D	system damping of area, pu MW/Hz
HVDC	High voltage direct current
MTDC	Multi terminal high voltage direct current
T_{SG}	speed governor time constant, s
T_T	steam turbine time constant, s
T_{PS}	power system time constant, s
R_{TH}	governor speed regulation parameters of thermal unit
R_{HY}	governor speed regulation parameters of hydro unit Hz/pu MW
R_G	governor speed regulation parameters of gas unit, Hz/pu MW
K_{PS}	power system gain, Hz/pu MW
K_R	steam turbine reheat constant
T_R	steam turbine reheat time constant, s
T_W	nominal starting time of water in penstock, s
T_{RS}	hydro turbine speed governor reset time, s
T_{RH}	hydro turbine speed governor transient droop time constant, s
T_{GH}	hydro turbine speed governor main servo time constant, s
X_G	lead time constant of gas turbine speed governor, s
Y_G	lag time constant of gas turbine speed governor, s
c_g	gas turbine valve positioner
b_g	gas turbine constant of valve positioner, s
T_F	gas turbine fuel time constant, s
T_{CR}	gas turbine combustion reaction time delay, s
T_{CD}	gas turbine compressor discharge volume-time constant, s
T_{WT}	Wind turbine time constant
T_{HVDC}	HVDC time constant

ACE	area control error
P_{rt}	rated capacity of the area, MW
f	nominal system frequency, Hz
D	system damping of area, pu MW/Hz
$HVDC$	High voltage direct current
$MTDC$	Multi terminal high voltage direct current
T_{SG}	speed governor time constant, s
T_T	steam turbine time constant, s
T_{PS}	power system time constant, s
R_{TH}	governor speed regulation parameters of thermal unit
R_{HY}	governor speed regulation parameters of hydro unit Hz/pu MW
R_G	governor speed regulation parameters of gas unit, Hz/pu MW
K_{PS}	power system gain, Hz/pu MW
K_R	steam turbine reheat constant
T_R	steam turbine reheat time constant, s
T_W	nominal starting time of water in penstock, s
T_{RS}	hydro turbine speed governor reset time, s
T_{RH}	hydro turbine speed governor transient droop time constant, s
T_{GH}	hydro turbine speed governor main servo time constant, s
X_G	lead time constant of gas turbine speed governor, s
Y_G	lag time constant of gas turbine speed governor, s
c_g	gas turbine valve positioner
b_g	gas turbine constant of valve positioner, s
T_F	gas turbine fuel time constant, s
T_{CR}	gas turbine combustion reaction time delay, s
T_{CD}	gas turbine compressor discharge volume-time constant, s
T_{WT}	Wind turbine time constant
T_{HVDC}	HVDC time constant

Appendix B: System parameters

$B_1 = B_2 = 0.4312$p. u. MW/Hz	$X_C = 0.6$ s
$P_{rt} = 2000$ MW	$Y_C = 1$ s
$P_L = 1840$ MW	$c_g = 1$
$R_1 = R_2 = R_3 = 2.4$ Hz/p. u.	$b_g = 0.05$ s
$R_{wt=}3.36$ Hz/p. u.	$T_F = 0.23\ s$
$T_{SG} = 0.08$ s	$T_{CR} = 0.01\ s$
$T_T = 0.3$ s	$T_{CD} = 0.2\ s$
$K_R = 0.3$ s	$T_{WT} = 1.5\ s$
$T_R = 10$ s	$k = 10.38$
$K_{PS1} = 68.9566$ Hz/p. u. MW	$K_T = 0.4347$
$K_{PS2} = 68.9566$ Hz/p. u. MW	$K_{HY} = 0.2608$
$T_{PS1} = T_{PS2} = 11.49$ s	$K_G = 0.1045$
$T_{12} = 0.0433$	$K_{WF} = 0.20$
$T_W = 1$ s	$K_{DC} = 1$
$T_{RS} = 5$ s	$T_{DC} = 0.2\ s$
$T_{RH} = 28.75$ s	$T_{HVDC} = 0.7\ s$
$T_{GH} = 0.2$ s	